Journal of Applied Electrochemistry 32: 763–773, 2002.
© 2002 Kluwer Academic Publishers. Printed in the Netherlands.



# Voltammetric and morphological characterization of copper electrodeposition from non-cyanide electrolyte

M.R.H. DE ALMEIDA[1], I.A. CARLOS[1,*], L.L. BARBOSA[1], R.M. CARLOS[2], B.S. LIMA-NETO[2] and E.M.J.A. PALLONE[3]
[1]*Departamento de Química, Universidade Federal de São Carlos, CP 676, 13565-905, São Carlos-SP, Brazil*
[2]*Instituto de Química de São Carlos, USP, São Carlos-SP, Brazil*
[3]*Departamento de Engenharia de Materiais, UFSCar, São Carlos-SP, Brazil*
*(*author for correspondence, e-mail: ivani@dq.ufscar.br)*

Received 21 September 2001; accepted in revised form 27 March 2002

*Key words:* AISI 1010 steel electroplating, copper, glycerol, non-cyanide bath, sulfate

**Abstract**

The electrodeposition of copper onto AISI 1010 steel using an alkaline electrolyte based on glycerol has been studied. The influence of NaOH concentration and the addition of sulfate as supporting electrolyte were investigated by voltammetric techniques. For a NaOH concentration $\geqslant 0.6$ M the plating bath was stable and immersion deposition onto steel was avoided. Voltammetric studies and SEM analysis indicated that the reduction process occurs through two different copper(II) species. The copper films were golden in colour, even in the high hydrogen evolution region, indicating that glycerinate anions prevent the copper deposits becoming darker. The presence of the sulfate anions affected the morphology of the copper films, acting as brighteners.

## 1. Introduction

Electrodeposition of copper from cyanide solutions is a long-established industrial practice [1–9]. The brighteners, adherence and colour of the deposits can be readily controlled by manipulating the experimental conditions [1]. Despite the high quality of the deposits obtained from the alkaline cyanide bath, this process is now used infrequently, not only because of its toxicity but also due to photoresistive attack during the plating process. Thus, an extensive search has been made for satisfactory alternative electrolytes. Much of this work has grown around electrolytic solutions of fluoborate [5, 6], pyrophosphate [1–3], acid sulfate [10–14], EDTA [15–23], citrate [24, 25], ammonia [26], ethylenediamine/ammonia [27], and glycerol/formaldehyde [28]. However, each of these electrolytes has limitations, such as corrosion attack, contamination by organic impurities and catalytic copper production [28].

We have been interested in the electrodeposition of copper on to AISI 1010 steel since we observed that the presence of additives in the plating bath had a beneficial effect on Cu/Sn and Pb electrodeposits [29, 30]. These studies demonstrated that the additives tartrate in the Cu/Sn and glycerol in the Pb plating baths inhibit strain and dendritic growth, respectively. In this context, we have undertaken a complete study of copper electrodeposition on AISI 1010 steel in glycerol solutions at various NaOH concentrations. The work described here illustrates how the glycerinate and sulfate anions can modify the morphology and brighteners of the copper electrodeposits. Understanding the dynamics of these processes is essential in the design of chemical systems for practical applications.

## 2. Experimental details

All chemicals were analytical grade. Double-distilled water was used throughout. The electrochemical experiment was performed in a freshly prepared non-cyanide bath, containing 0.10 M $CuSO_4$, 0.20 M glycerol and NaOH at various concentrations (0.40, 0.60, 1.0, 2.0 and 3.0 M), in the absence and presence of $Na_2SO_4$ as supporting electrolyte. An AISI 1010 steel disc (0.50 $cm^2$), a Pt plate and an appropriate Lugging capillary containing Hg/HgO/NaOH (1.0 M), were employed as working, auxiliary and reference electrodes, respectively. Where indicated, a Cu disc electrode (0.28 $cm^2$) replaced the AISI 1010 steel. The AISI 1010 steel (CSN Co., Brazil) contained 0.04% P, 0.08% C, 0.3% Mn and 0.05% S. Immediately prior to the electrochemical measurements, the working electrode was ground with 600 emery paper and rinsed with distilled water. Potentiodynamic curves were recorded using an EG&G electrochemical system consisting of a model 366A bipotentiostat. Measurements of deposition and dissolution charges were recorded with an EG&G

model 379 coulometer. All experiments were carried out at room temperature (25 °C).

The deposition current efficiency ($\phi_e$) of the chronoamperometric copper electrodeposition process was obtained from the stripping/deposition charge ratio. The copper films were obtained chronoamperometrically from −0.3 V to various deposition potentials ($E_d$), at a charge density ($q_d$) of 0.4 C $cm^{-2}$.

The anodic stripping was done in various solutions of identical molarity (1.0 M): $NH_4Cl$, $(NH_4)_2SO_4$, $NaNO_3$ and $NH_4NO_3$. The best results were obtained with $NH_4NO_3$ and $NaNO_3$, and $NH_4NO_3$ was chosen owing to the lower passivation charge on the AISI 1010 steel. The other solutions corroded the steel substrate and so proved unsuitable. Scanning electron microscopy (SEM) photographs were taken with an FEG X L 30. The deposition baths were analysed by u.v.–vis. molecular absorption spectrophotometry, using an HP 8453 Spectrophotometer, and by potentiometric titration, using a Micronal B474 pH meter. Energy dispersive X-ray spectroscopy (EDS) measurements were made with a Zeiss/Leica (model LEO 440) EDS Si/Li, with Be ultrathin window.

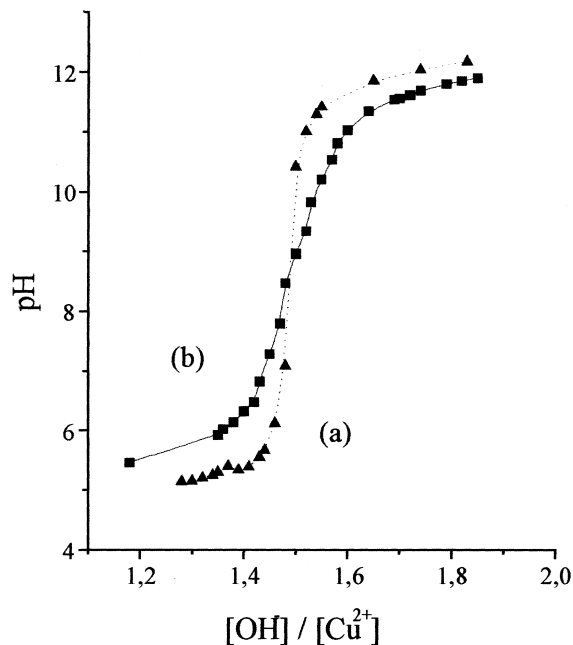


*Fig. 1.* Formation curves for the copper(II): (a) dimers (●) and (b) complexes (■), obtained by potentiometric titration of (a) 0.10 M $CuSO_4$ and (b) 0.10 M $CuSO_4$/0.20 M glycerol, with 0.099 00 M NaOH.

## 3. Results and discussion

### 3.1. *Deposition bath stability and immersion deposition*

AISI 1010 steel plates were immersed in the copper/glycerol solutions at various NaOH concentrations (0.20–3.0 M) to test immersion deposition of copper onto steel. With regard to solution stability, it was observed that the solutions at NaOH concentrations higher than 0.20 M were of a clear deep blue colour, without precipitate. At NaOH concentrations $\leqslant 0.20$ M, feeble immersion deposits of copper were generated on the immersed steel by the displacement of copper ions in the solution. As a consequence, adhesion of subsequently plated layers was hindered. Although small, the dissolution of the steel substrate during immersion deposition contributed to bath contamination.

Figures 1(a) and (b) show the potentiometric titration curves of $CuSO_4$ with NaOH in the absence and presence of glycerol, respectively.

During the titration of 0.10 M $CuSO_4$ with 0.099 00 M NaOH (Figure 1(a)), the crystalline blue solution turned dark green, owing to precipitation of $Cu^{2+}$. The curve exhibits only one end-point at a $OH^-$ to $Cu^{2+}$ molar ratio of 3:2, indicating the presence of the dimer $[Cu_2(OH)_3]^+$ [31] (Equation 1).

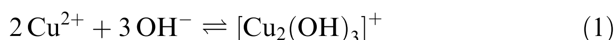

$$2\,Cu^{2+} + 3\,OH^- \rightleftharpoons [Cu_2(OH)_3]^+ \qquad (1)$$

During the titration of 0.10 M $CuSO_4$ and 0.20 M glycerol with 0.099 00 M NaOH (Figure 1(b)), the crystalline blue solution turned pale blue with formation of a white precipitate. In this reaction step, an end-point was obtained only when the $OH^-/Cu^{2+}$ ratio was 3:2, corresponding to the formation of the complex $Cu_2(OH)(glyc)_2^+$. This process involves the loss of two protons per glycerol ligand, as in Equation 2:

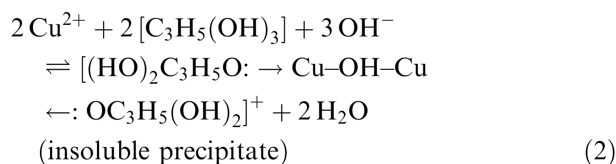

$$2\,Cu^{2+} + 2\,[C_3H_5(OH)_3] + 3\,OH^- \rightleftharpoons [(HO)_2C_3H_5O{:} \rightarrow Cu\text{–}OH\text{–}Cu \leftarrow{:}\, OC_3H_5(OH)_2]^+ + 2\,H_2O \text{ (insoluble precipitate)} \qquad (2)$$

Continuous addition of base beyond the end-point turned the solution intense blue, with complete dissolution of the precipitate, suggesting the formation of the complexes Cu(glyc) (**A**) and $[Cu(glyc)_2]^{2-}$ (**B**) (Equations 3 and 4), respectively.

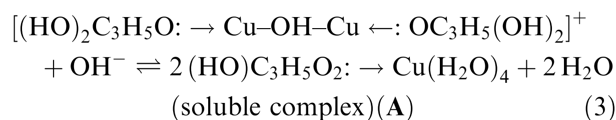

$$[(HO)_2C_3H_5O{:} \rightarrow Cu\text{–}OH\text{–}Cu \leftarrow{:}\, OC_3H_5(OH)_2]^+ + OH^- \rightleftharpoons 2\,(HO)C_3H_5O_2{:} \rightarrow Cu(H_2O)_4 + 2\,H_2O \text{ (soluble complex)}(\mathbf{A}) \qquad (3)$$

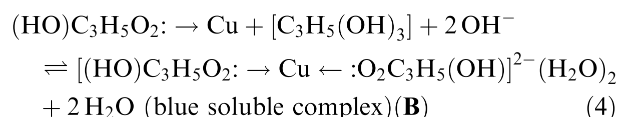

$$(HO)C_3H_5O_2{:} \rightarrow Cu + [C_3H_5(OH)_3] + 2\,OH^- \rightleftharpoons [(HO)C_3H_5O_2{:} \rightarrow Cu \leftarrow {:}O_2C_3H_5(OH)]^{2-}(H_2O)_2 + 2\,H_2O \text{ (blue soluble complex)}(\mathbf{B}) \qquad (4)$$

These results corroborate those obtained by Koyano who studied an electroless copper bath containing glycerol/formaldehyde [28]. The endpoint ratio $[OH^-]/[Cu^{2+}] = 1.5$ was obtained during titration of $CuSO_4$/glycerin with NaOH, corresponding to the formation of the complex $Cu_2(OH)(glyc)_2^+$ (Equation 2) which, by dissolution with NaOH, becomes **A** and **B**.

The thermodynamics of metal complex formation has been discussed by Pearson [32] in terms of hard and soft acids and bases [33]. The $Cu^{2+}$ ion is on the borderline between hard and soft. Consequently $Cu^{2+}$ ions react preferentially with hard bases. As the glycerinate ion is a harder base than $OH^-$, the $Cu^{2+}$/glycerinate complexes, **A** and **B**, will be more stable thermodynamically than the $Cu^{2+}/OH^-$ complex.

Also, the presence in the plating bath of two such complexes, possessing different geometry, are consistent with the electronic configuration of the $Cu^{2+}$ ion, [Ar] $3d^9$, which leads to the formation of complexes of differing geometry in solution. Moreover, the formation of the two different ion complexes (**A** and **B**) in solution, proposed in these experiments, was corroborated by the electronic absorption spectrum results outlined below.

### 3.2. *Absorption spectra*

Figure 2 shows the electronic absorption characteristics of the copper(II) complexes. Figure 2(a) shows the spectrum of 0.025 M $CuSO_4$ in aqueous solution and Figure 2(b) that of $1.3 \times 10^{-4}$ M Cu(II) solution in the presence of $2.6 \times 10^{-4}$ M glycerol and $7.8 \times 10^{-4}$ M NaOH, in the wavelength region 400–1200 nm. Figure 2 clearly shows that the change of ligand has a strong influence on the positions of the absorption maxima of the copper(II) complexes. When changing from aquo to glycerinate ligand, the single absorption band at 814 nm splits into a peak at 630 nm and a shoulder at 550 nm. The intensity of the lowest energy absorption band of these complexes increases on going from aquo to glycerinate ligand. The absorption maximum observed in Figure 2(b) is characteristic of the absorption spectra of copper(II) coordination complexes where copper(II) is attached to four oxygen atoms. Similar absorption spectra have been observed with the catechol ligand [34], whose absorption spectra are characterized by a large band of low intensity, typical of a d–d transition, at approximately 700 nm and a ligand to metal charge-transfer transition band of high intensity, at ~440 nm.

The formation of the Cu(II)-glycerinate complexes explains why their absorption spectra differ from that of Cu $(H_2O)_6^{2+}$, Figure 2(a), which shows only a single, composite charge transfer band at low energy.

### 3.3. *Electrochemical study in the absence of sulfate*

Figure 3 shows linear sweep voltammograms recorded from the AISI 1010 steel substrate in copper/glycerol solutions at various NaOH concentrations (0.40–3.0 M). The two cathodic peaks ($c_1$, $c_2$) are attributed to reduction of the two Cu(II) complexes ions (Cu(glyc) and $[Cu(glyc)_2]^{2-}$). In addition, the increase in the current density beyond cathodic peak $c_2$ can be associated with hydrogen evolution. It can be observed in Figure 3, that the copper plating rate is affected kinetically by the hydroxide ion. The cathodic current density in the region of peak $c_2$ increased significantly when the $OH^-$ concentration went above 1.0 M, due probably to the higher concentration of complex **B** with respect to complex **A**. Moreover, it has been observed that the hydroxide ion affects the plating thermodynamically. In the range of NaOH concentration (0.40–3.0 M) the complex Cu(glyc), which is less stable than $[Cu(glyc)_2]^{2-}$, is reduced in the region of peak $c_1$, while $[Cu(glyc)_2]^{2-}$ in the region of peak $c_2$. Figure 3 and Table 1 show that the variation of the deposition potentials of peaks $c_1$ with NaOH concentration is insignificant, while in the region of $E_{pc2}$ a shift of more than 100 mV in the negative direction can be seen (Table 1), for the 3.0 M NaOH concentration in relation to 0.4–0.6 M NaOH. This is probably due to the high-limit diffusional control in this region, since the complex **A** concentration

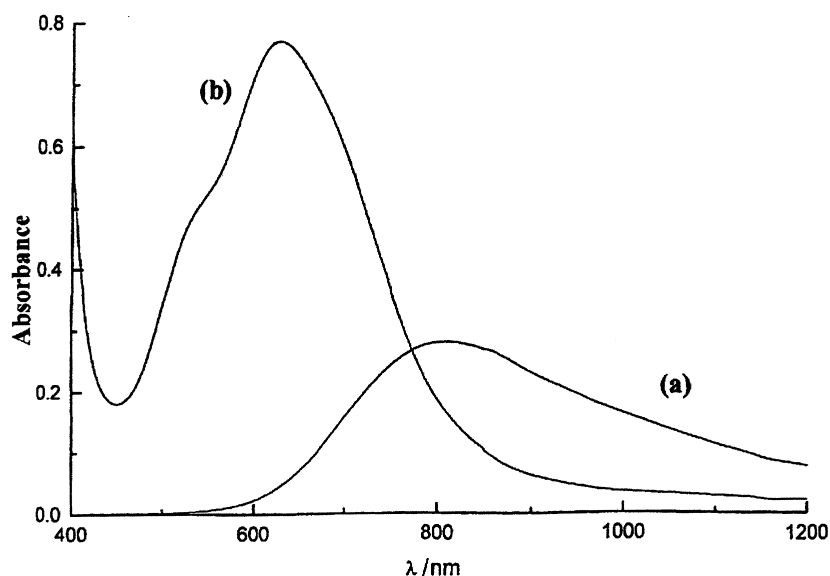


*Fig. 2.* Absorption spectra of the electrolyte solutions: (a) 0.025 M $CuSO_4$, (b) $1.3 \times 10^{-4}$ M $CuSO_4$, $2.6 \times 10^{-4}$ M glycerol and $7.8 \times 10^{-4}$ M NaOH.

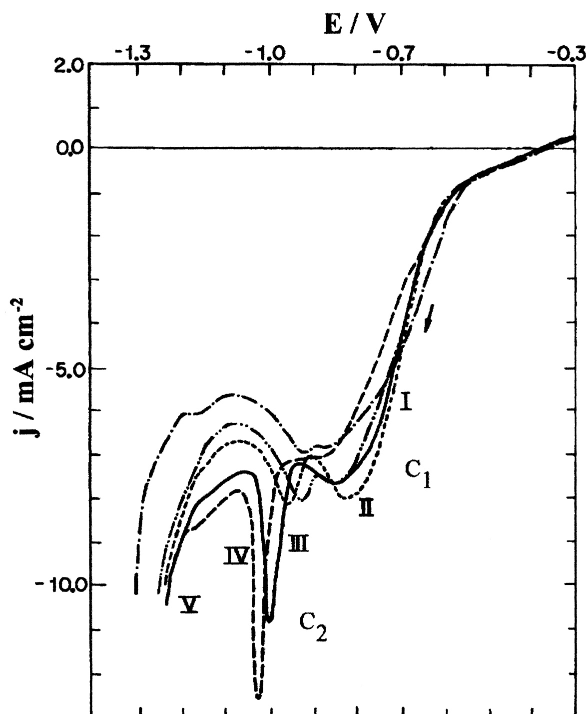


*Fig. 3.* Voltammetric curves for steel substrate in 0.10 M $CuSO_4$ and 0.20 M glycerol, for various NaOH concentrations: (– • –) 0.4; (– •• –) 0.6; (- - -) 1.0 M; (—) 2.0 and (– – –) 3.0 M, at 10 mV $s^{-1}$.

*Table 1.* Observed cathodic peak potentials ($E_{pc}$) and cathodic peak current densities ($j_{pc}$) from copper voltametric deposition obtained in the *absence* of sulfate

| $[OH^-]$/M | $E_{pc1}$/V | $j_{pc1}$/mA $cm^{-2}$ | $E_{pc2}$/V | $j_{pc2}$/mA $cm^{-2}$ |
|---|---|---|---|---|
| 0.4 | −0.84 | −6.8 | −0.92 | −7.0 |
| 0.6 | −0.84 | −7.6 | −0.93 | −8.0 |
| 1.0 | −0.82 | −8.0 | −0.96 | −8.1 |
| 2.0 | −0.84 | −7.7 | −1.00 | −10.8 |
| 3.0 | −0.89 | −7.1 | −1.03 | −12.6 |

decreases and the formation of complex **B** is favoured with increasing NaOH concentration, as discussed above. It may be inferred from these results that in the region of $E_{pc1}$ and $E_{pc2}$ the reducing species are always the same, Cu(glyc) and $[Cu(glyc)_2]^{2-}$, respectively.

Bearing in mind that the electrode surface composition undergoes a continuous change during the cathodic deposition, AISI 1010 steel and copper electrodes were studied to obtain their hydrogen evolution overpotentials, in the glycerol solutions at various NaOH concentrations, without the plating salt.

Figure 4 shows typical cathodic voltammograms for AISI 1010 steel and copper electrodes. Figure 4(a) and (b) show that, while the $H_2$ evolution reaction on the steel substrate starts from the initial stage of the plating process, on the copper electrode the $H_2$ evolution is significant only at potentials beyond −1.1 V. These results allow the different substrates to be ranked in the order: copper > AISI 1010 steel, according to their hydrogen evolution potentials, approximately −1.2 V and −0.7 V, respectively. An interesting feature of the copper substrate (Figure 4(b)) is that the three cathodic peaks on the forward cathodic scan can be associated with the reduction of the copper oxides produced at the beginning of potential scan (−0.3 V) [35]. Beyond these peaks, the current density increases steeply, due to the hydrogen evolution. Figure 4($b_1$) shows the voltammogram of a copper electrode in 0.6 M NaOH solution, without glycerol. The three cathodic peaks arising from the reduction of the copper oxides are again produced, corroborating the above results. These results accord with our previous observation that glycerol reduction does not occur [30, 36].

Figure 5 illustrates the effect of increasing the $OH^-$ ion concentration on the current efficiency ($\phi_e$) of the chronoamperometric copper deposition process. The copper films were obtained chronoamperometrically from −0.30 V to various $E_d$, at a $q_d$ of 0.4 C $cm^{-2}$. It

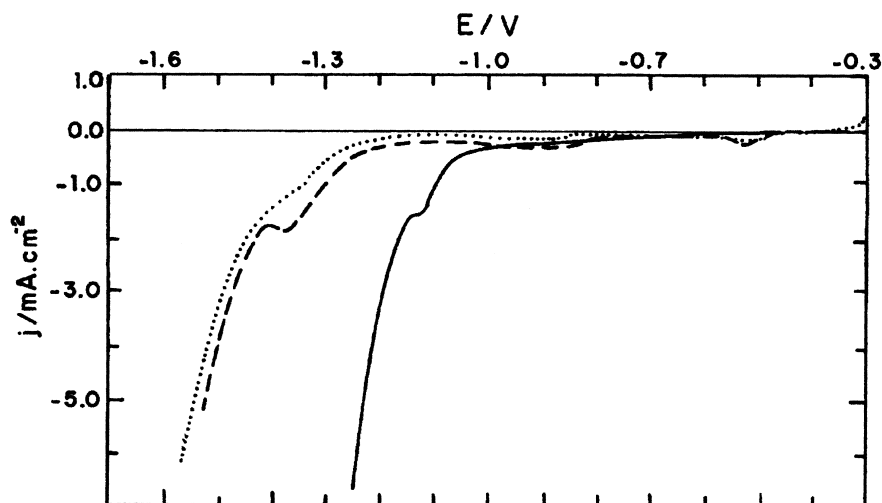


*Fig. 4.* Voltammetric curves for: (a) AISI 1010 steel (—) and (b) copper (- - -) electrodes in 0.20 M $C_3H_8O_3$/0.60 M NaOH; ($b_1$) copper (– – –) electrode in 0.60 M NaOH, at 10 mV $s^{-1}$.

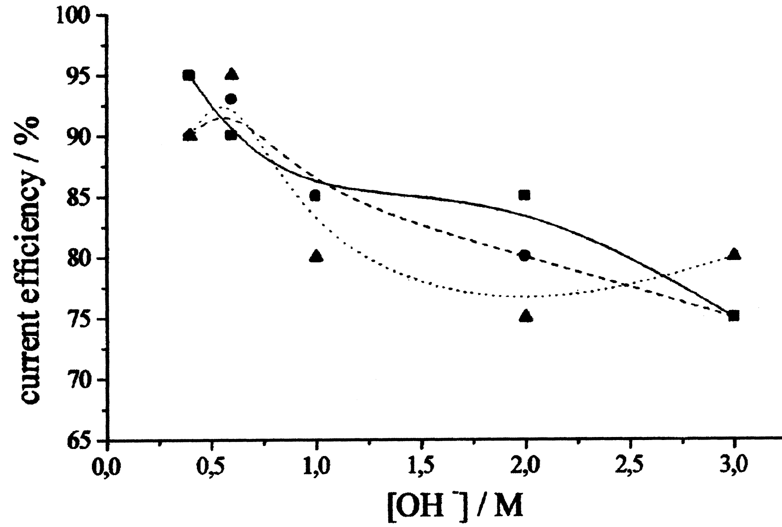


*Fig. 5.* Copper deposition current efficiency ($\phi_e$) at several deposition potentials ($E_d$): −1.0 (●), −0.85 (■) and −0.70 V (▲), against various NaOH concentrations.

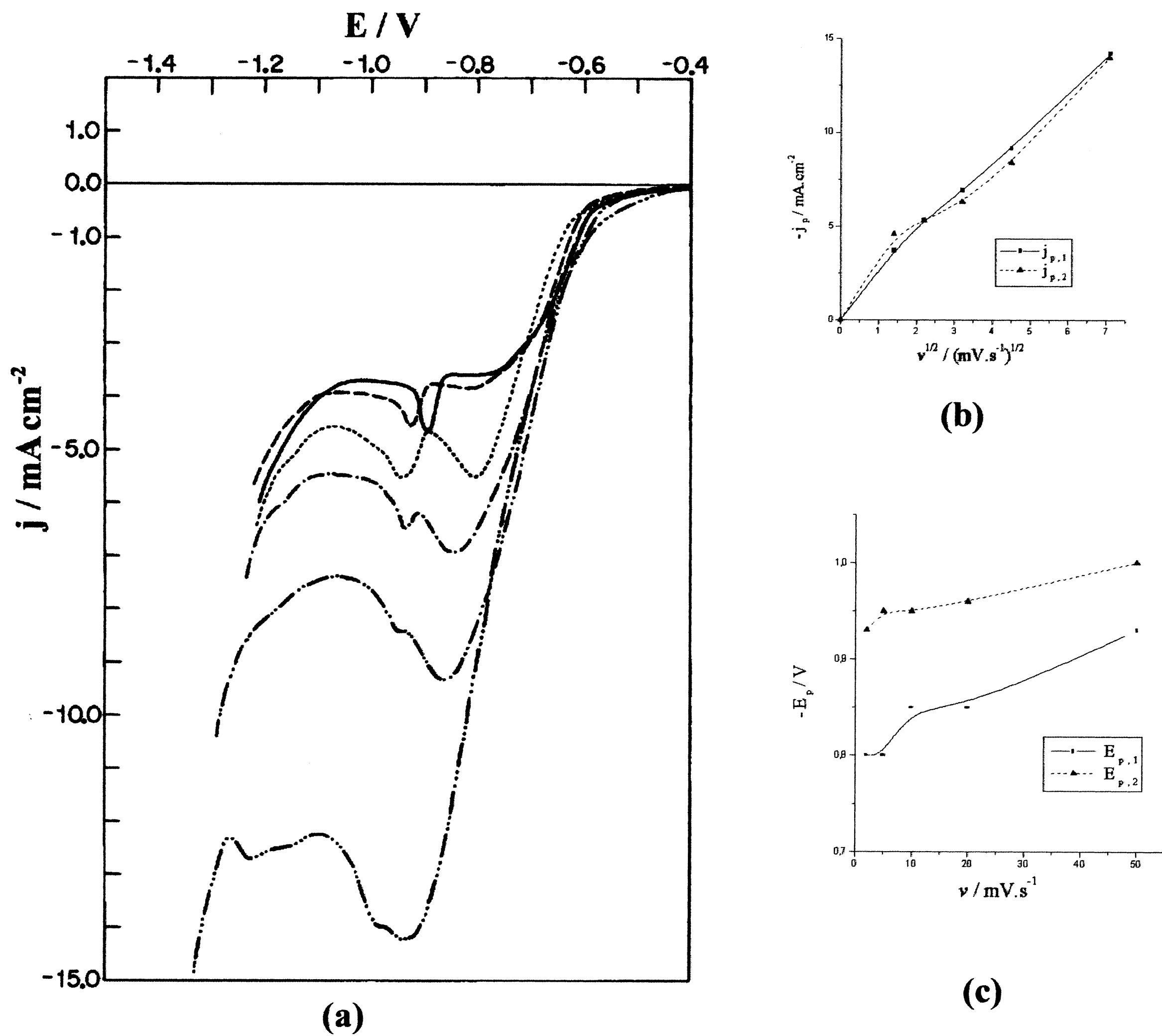


*Fig. 6.* (a) Voltammetric curves for AISI 1010 steel substrates in 0.10 M $CuSO_4$, 0.20 M $C_3H_8O_3$ and 0.60 M NaOH, at various sweep rates ($v$/mV $s^{-1}$): (—) 1.0; (– – –) 2.0; (- - -) 5.0; (– • –) 10; (– •• –) 20; (– • • • –) 50; (b) variation of $j_p$ with $v^{1/2}$ and (c) variation of $E_p$ with $v$, for copper electrodeposition on steel substrate.

can be seen that decreasing the NaOH concentration increases the $\phi_e$ values. Also, they are lower than 100%, denoting simultaneous discharge of hydrogen. These results agree with those obtained in Figures 4(a) and (b). Thus, the best $\phi_e$ values ($\geqslant$85%) were observed in the baths containing 0.40 and 0.60 M NaOH, at the deposition potentials of −0.70 to −1.0 V. After approximately a month, the bath containing 0.40 M NaOH becomes unstable, with formation of a red powder, probably copper(I) oxide.

To gain more insight into the proposed mechanism, a set of voltammograms at different sweep rates ($v$) was taken. Figure 6(a) shows a significant increase in the current densities of both peaks $c_1$ and $c_2$ with rising $v$, and not only in that of peak $c_1$. The latter would be expected if the deposition process had occurred through Cu(II) to Cu(I) species (peak $c_1$) and Cu(I) to Cu(O) (peak $c_2$). Figure 6(b) shows that peak current density ($j_p$) increases with $v^{1/2}$, but is not proportional. This result suggests that the copper electrodeposition process is quasi-reversible in this region [37–39]. Figure 6(c) shows that peak potential ($E_p$) shifts negatively with increasing $v$, confirming the results of Figure 6(b) [37–39].

Copper electrodeposition studies using a rotating disk electrode (Figure 7(a)) were carried out and the results show that the deposition process is controlled by mass transport. This can be seen more clearly in Figure 7(b).

The evidence above indicates that peaks $c_1$ and $c_2$ are related to the two Cu(II) complexes **A** and **B**, and this was confirmed by reversed cathodic sweeps at various potentials, and SEM photomicrographs, as can be verified in the discussion of Figures 9, 10(a) and 12(a) as explained in subsequent sections.

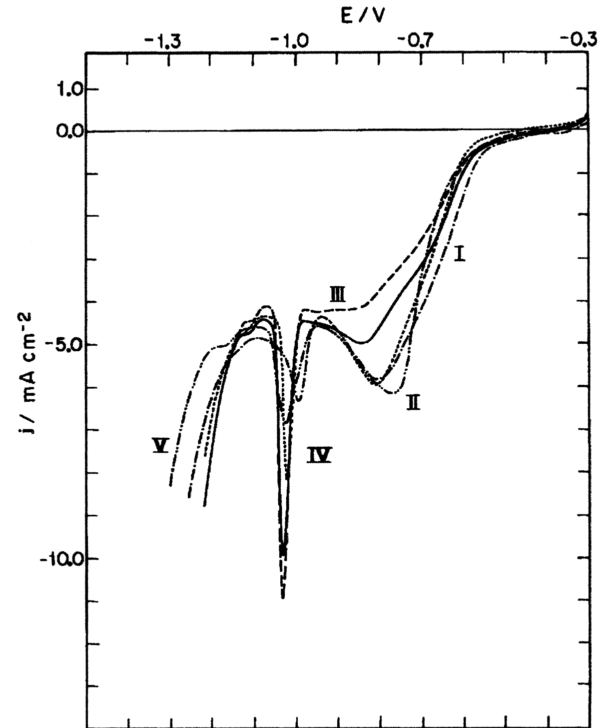


*Fig. 8.* Voltammetric curves for steel substrate in 0.10 M $CuSO_4$, 0.20 M glycerol, 1.0 M $Na_2SO_4$, for various NaOH concentrations: (– • –) 0.4, (– •• –) 0.6, (- - -) 1.0, (—) 2.0 and (– –) 3.0 M, at 10 mV $s^{-1}$.

### 3.4. *Electrochemical study in the presence of sulfate*

Figure 8 shows voltammetric curves for the AISI 1010 steel electrode in the copper plating bath at several

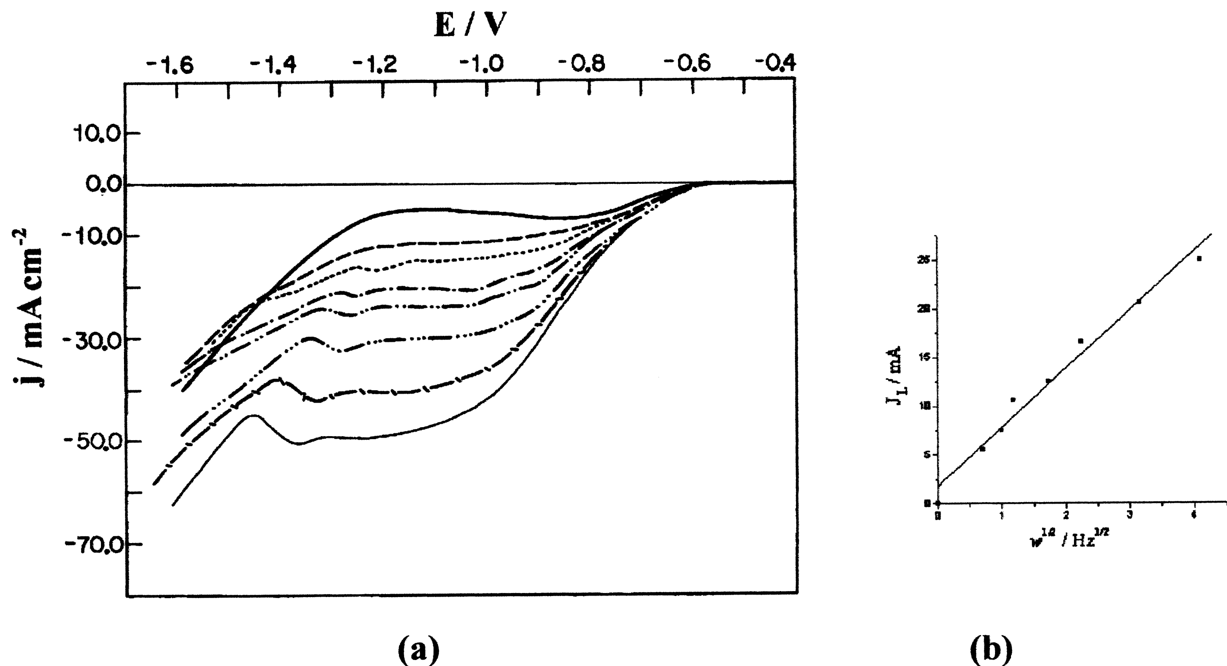


*Fig. 7.* (a) Voltammetric curves for rotating AISI 1010 steel substrates in 0.10 M $CuSO_4$, 0.20 M $C_3H_8O_3$ and 0.60 M NaOH, at various rotation speeds ($w$/Hz): (—) 0.0; (– – –) 0.5; (- - -) 1.0; (– • –) 2.0; (– • –) 3.0; (– • • • –) 5.0; (–/–) 10.0; (—) 16.7; (b) variation of $j_L$ with $w^{1/2}$ for copper electrodeposition onto steel RDE.

*Table 2.* Observed cathodic peak potentials ($E_{pc}$) and cathodic peak current densities ($j_{pc}$) from copper voltametric deposition obtained in the *presence* of sulfate

| $[OH^-]$/M | $E_{pc1}$/V | $j_{pc1}$/mA cm$^{-2}$ | $E_{pc2}$/V | $j_{pc2}$/mA cm$^{-2}$ |
|---|---|---|---|---|
| 0.4 | −0.80 | −5.9 | −1.00 | −6.4 |
| 0.6 | −0.76 | −6.2 | −1.02 | −6.9 |
| 1.0 | −0.80 | −6.0 | −1.02 | −8.2 |
| 2.0 | −0.84 | −5.0 | −1.03 | −10.0 |
| 3.0 | −0.85 | −4.3 | −1.03 | −11.0 |

NaOH concentrations in the presence of sodium sulfate. The presence of sulfate anions does not shift the deposition potentials significantly, but reduces the deposition current density (Table 2), indicating that the contribution of the migrational component to the copper deposition was eliminated.

The $H_2$ evolution overpotentials for the AISI 1010 steel and Cu electrodes, with sulfate anions present in the plating bath, were similar to those without sulfate (Figures 4(a) and (b)).

The effect of increasing the $OH^-$ ion concentration on the electrochemical efficiency ($\phi_e$) was studied. The copper films were obtained chronoamperometrically from −0.30 V to various $E_d$, with $q_d$ of 0.4 C cm$^{-2}$. The results obtained were similar to those without sulfate. Also, as in the absence of sulfate, the best values of $\phi_e(\geqslant 90\%)$ were observed in the baths containing 0.40 and 0.60 M NaOH in the $E_d$ range from −0.6 to −1.0 V.

Thus, the plating bath containing 0.60 M NaOH was chosen for further studies of copper deposition in the presence of sulfate.

Copper electrodeposition studies at various sweep rates using a stationary electrode, and various rotation rates using a rotating disc electrode (RDE), were similar to those without sulfate. The diffusion coefficient ($D_0$) of the copper complexes was obtained through RDE studies. Assuming a kinematic viscosity of 0.01 cm$^2$ s$^{-1}$, and a roughness factor of about 2 (AISI 1010 steel substrate), the value of the diffusion coefficient was $3.5 \times 10^{-6}$ cm$^2$ s$^{-1}$. This value, as expected, is smaller than the $D_0$ of copper sulfate, $7 \times 10^{-6}$ cm$^2$ s$^{-1}$ [40], but is comparable to that of copper complexes such as the copper–EDTA complex, $(3–4) \times 10^{-6}$ cm$^2$ s$^{-1}$ [41] and a copper–citrate complex, $2.1 \times 10^{-6}$ cm$^2$ s$^{-1}$ [41].

The analysis of the voltammetric deposition from 0.10 M $CuSO_4$, 0.20 M glycerol, 0.60 M NaOH and 1.0 M $Na_2SO_4$ solution, becomes clearer when the cathodic sweep is reversed at various potentials (Figure 9). At potentials lower than −0.60 V (dotted line), the cathodic current increases and a nucleation loop is observed, suggesting that the metal deposition occurs by nucleation [29, 42]. When the sweep was reversed at approximately −0.80 V (solid line), the current decreased, indicating that the plating process kinetics is controlled by diffusion [29, 37]. Finally, when the sweep was reversed at potentials more negative than −1.20 V (broken line), the current also decreased, indicating that the area of copper electrodeposit had not increased.

For the anodic processes, the peak $a_1$ increased as the amount of deposited metal increased, since the cathodic sweep was reversed at a more negative potential each time. The nucleation loop at −0.6 V in the cathodic sweep, and the dissolution peak $a_1$ in the anodic sweep, indicate the existence of copper crystallites. These results are in agreement with the reduction of two different Cu(II) species (**A** and **B**), Equations 3 and 4, proposed above.

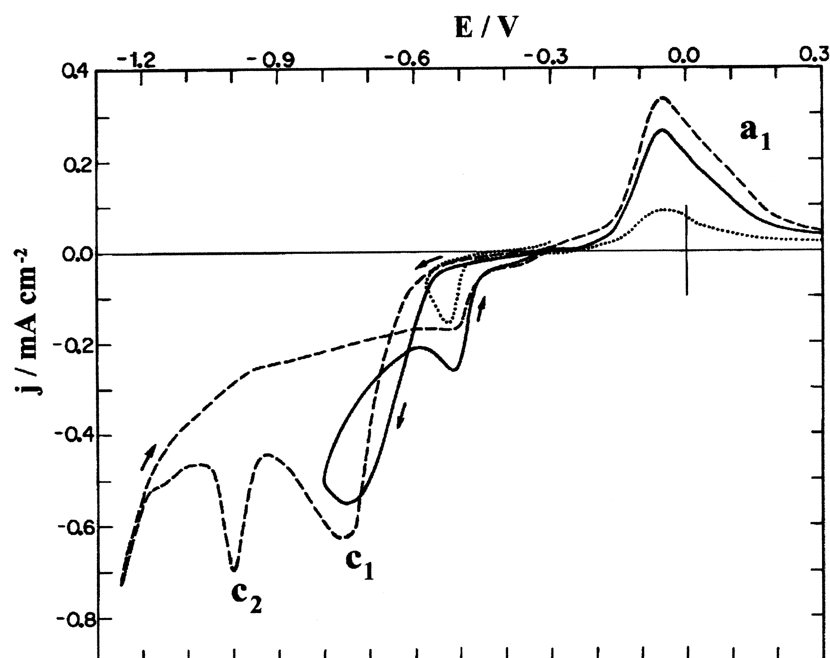


*Fig. 9.* Voltammetric curves for steel substrates in 0.10 M $CuSO_4$, 0.20 M $C_3H_8O_3$, 0.60 M NaOH and 1.0 M $Na_2SO_4$; effect of the limit potentials: (- - -) −0.60, (—) −0.80 and (– – –) −1.25 V.

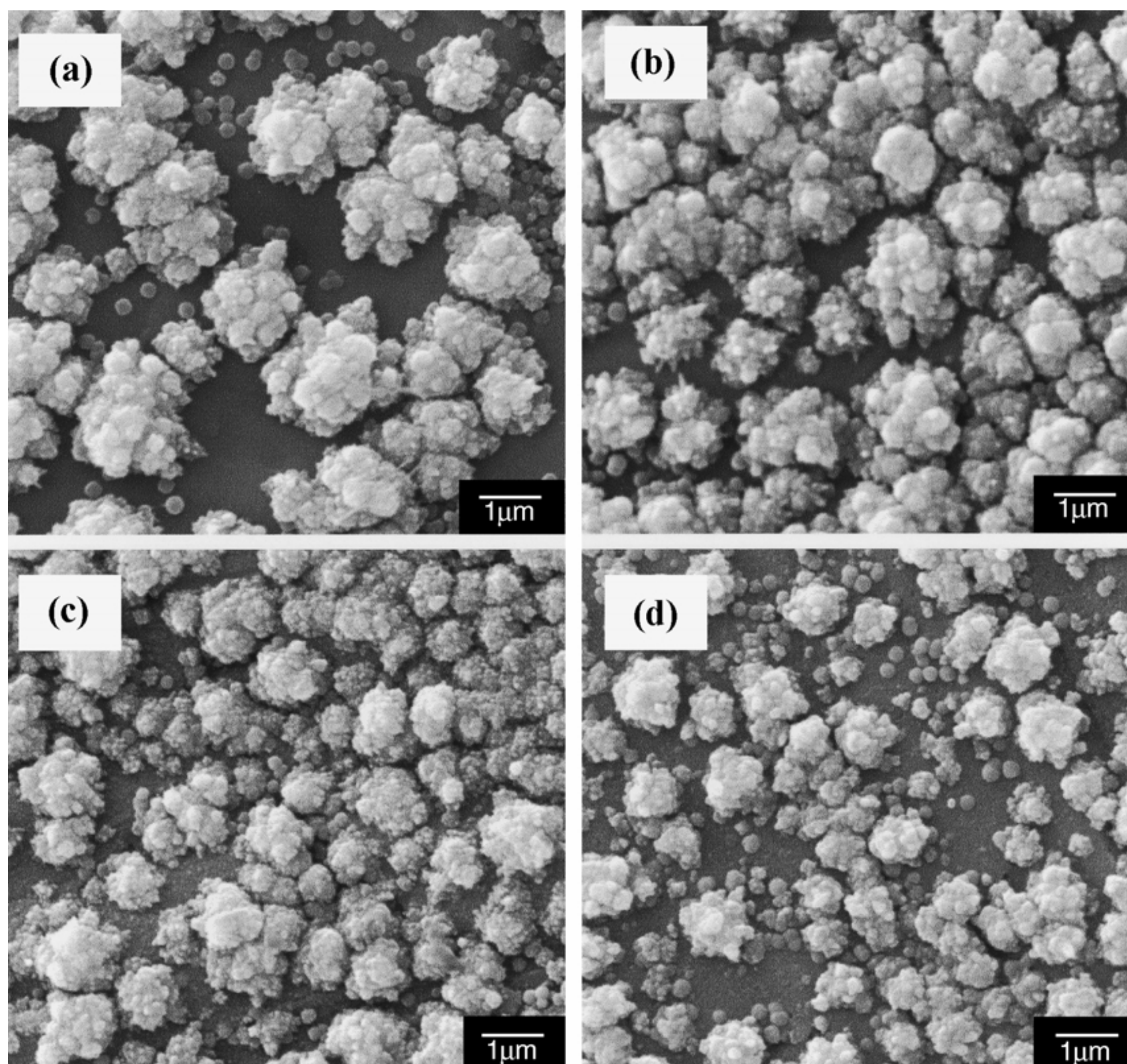


*Fig. 10*. SEM micrographs for Cu films of 0.6 C $cm^{-2}$ obtained in different hold potentials defined in Figure 3: (a) −0.69, (b) −0.75, (c) −1.0, and (d) −1.28 V. Electrolytic solution: 0.10 M $CuSO_4$, 0.20 M $C_3H_8O_3$ and 0.60 M NaOH, at 10 mV $s^{-1}$.

### 3.5. *Morphological study*

A morphological study was carried out by scanning electron microscopy (SEM) to analyse the effects of the hold potential in the different zones of the voltammetric deposition curves and to establish the relationship between the deposition potential and film morphology.

Figures 10(a), (b), (c) and (d) show micrographs of the copper deposits of 0.6 C $cm^{-2}$, obtained in the absence of sulfate in the plating bath, with the hold potential in the different zones of the voltammetric curve, after scanning from −0.3 V to each hold potential. When the hold potential was taken at −0.69 V, small globular crystallites and large clusters covering the substrate were obtained (Figure 10(a)). Figures 10(b), (c) and (d) show the micrographs for hold potentials at −0.75, −0.93 and −1.28 V, during the voltammetric deposition (Figure 3), respectively. Increasingly negative potential, the size of clusters decreased gradually increasingly negative potential and the deposits obtained were clear and golden, even at more negative potentials. These results are in accord with the 3D nucleation and growth mechanism.

The influence of potentials in the various zones of the voltammetric deposition curves was also analysed in the presence of sulfate. Copper films of 0.6 C $cm^{-2}$ were obtained at hold potentials in the various zones of the voltammetric curve (Figure 8), after scanning from −0.3 V to each hold potential. Figures 11(a), (b), (c) and (d) show the micrographs for hold potentials at −0.69, −0.75, −1.0 and −1.28 V, during the voltammetric deposition, respectively. The morphology of the copper deposits went from a homogeneous morphology (Figures 11(a) and (b)) to one composed of small coalesced crystallites and crystallite clusters dispersed on the substrate (Figures 11(c) and (d)). These copper deposits were always golden. The micrographs show that the sulfate anion decreases the size of the copper crystallites, starting from the deposition potential of about −0.69 V, suggesting that the sulfate anions act as brighteners. It can be inferred from these results that AISI 1010 steel substrate coverage by copper deposits

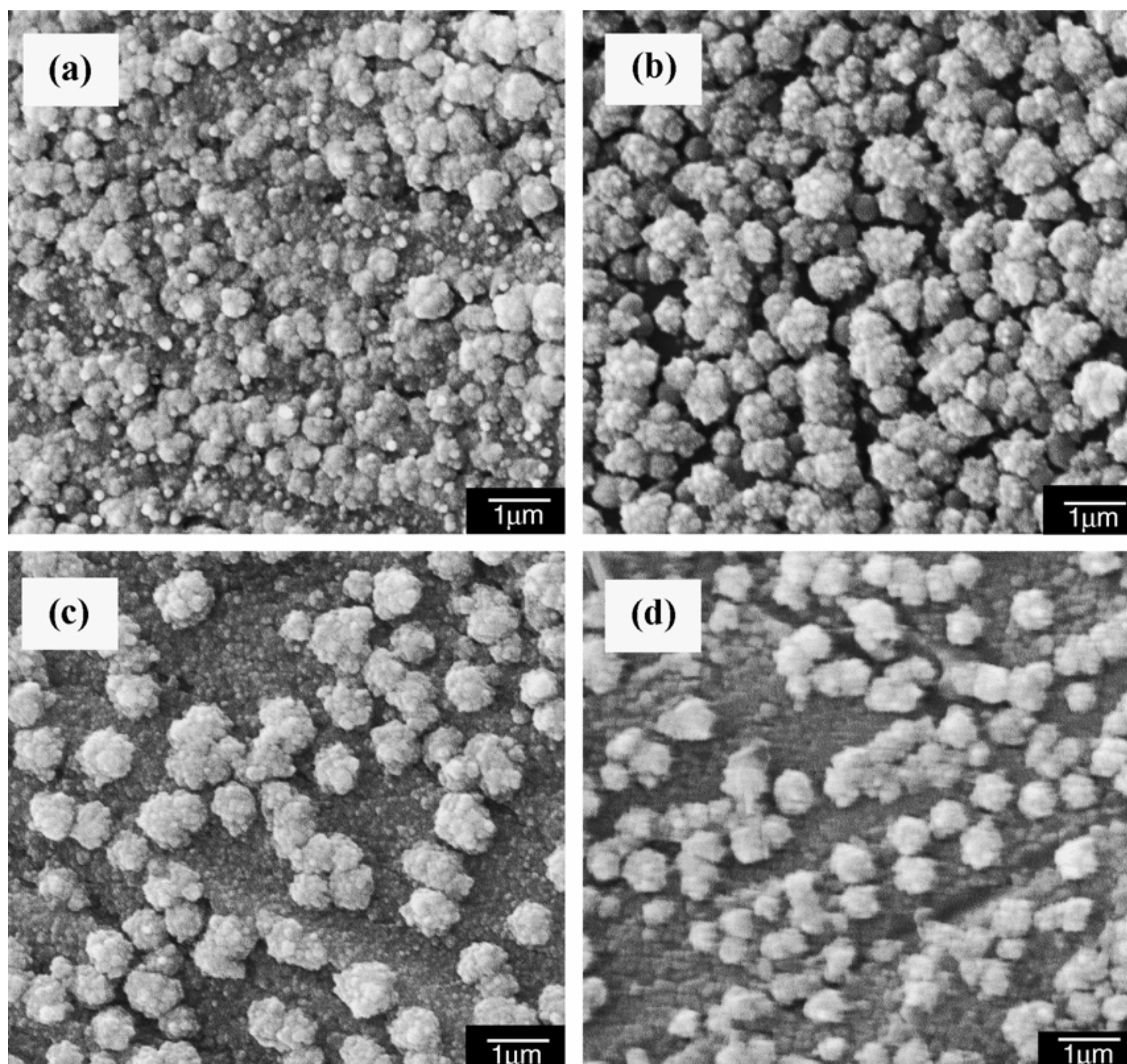


*Fig. 11.* SEM micrographs for Cu films of 0.6 C $cm^{-2}$ obtained from −0.3 V at different hold potentials defined in Figure 8: (a) −0.69, (b) −0.75, (c) −1.0 and (d) −1.28 V. Electrolytic solution: 0.10 M $CuSO_4$, 0.20 M $C_3H_8O_3$, 0.60 M NaOH and 1.0 M $Na_2SO_4$, at 10 mV $s^{-1}$.

was better in the presence of sulfate than in its absence in the plating bath.

Figures 12(a) and (a′) show micrographs of the copper deposits of 0.6 C $cm^{-2}$, obtained chronoamperometrically from −0.30 to −0.69 V in the absence and presence of sulfate, respectively. The sulfate anions refine the nodular crystallites. Figures 12(b) and (b′) show micrographs of the copper deposits obtained from −0.30 to −1.28 V. The negative high potential favours nucleation and small crystallites, which leads to good levelling. Also, gold-coloured films were observed.

These experiments show the existence of copper crystallites already at the beginning of peak $c_1$ (Figures 3 and 8), as proposed in the analysis of Figure 9, in accordance with a three-dimensional (3D) progressive nucleation mechanism. Also, this corroborates the proposed mechanism of reduction of copper from **A** (peak $c_1$) and **B** (peak $c_2$) copper(II) complexes.

EDS did not show the presence of carbon or sulfur in any copper deposited on to a Pt substrate, at −0.69 V and −1.28 V and charge density of 2 C $cm^{-2}$, either in the presence or absence of sulfate. These results indicate that glycerinate and sulfate anions are not incorporated into the deposit.

## 4. Conclusions

Golden copper electrodeposits were successfully obtained from 0.10 M $CuSO_4$, 0.20 M glycerol, 0.60 M NaOH and 1.0 M $Na_2SO_4$ solutions. For NaOH concentrations $\geqslant 0.60$ M the plating bath was stable and immersion deposition on AISI 1010 steel was avoided. The electrochemical efficiency was higher at lower NaOH concentration. SEM analysis and voltammetric studies corroborate the mechanism for the reduction process through two different Cu(II) complex ions (**A** and **B**). SEM analyses proved that the sulfate anions act as brighteners. The copper films were of a golden colour, even in the region of high hydrogen evolution, suggesting that glycerinate anions prevent the deposits becoming darker.

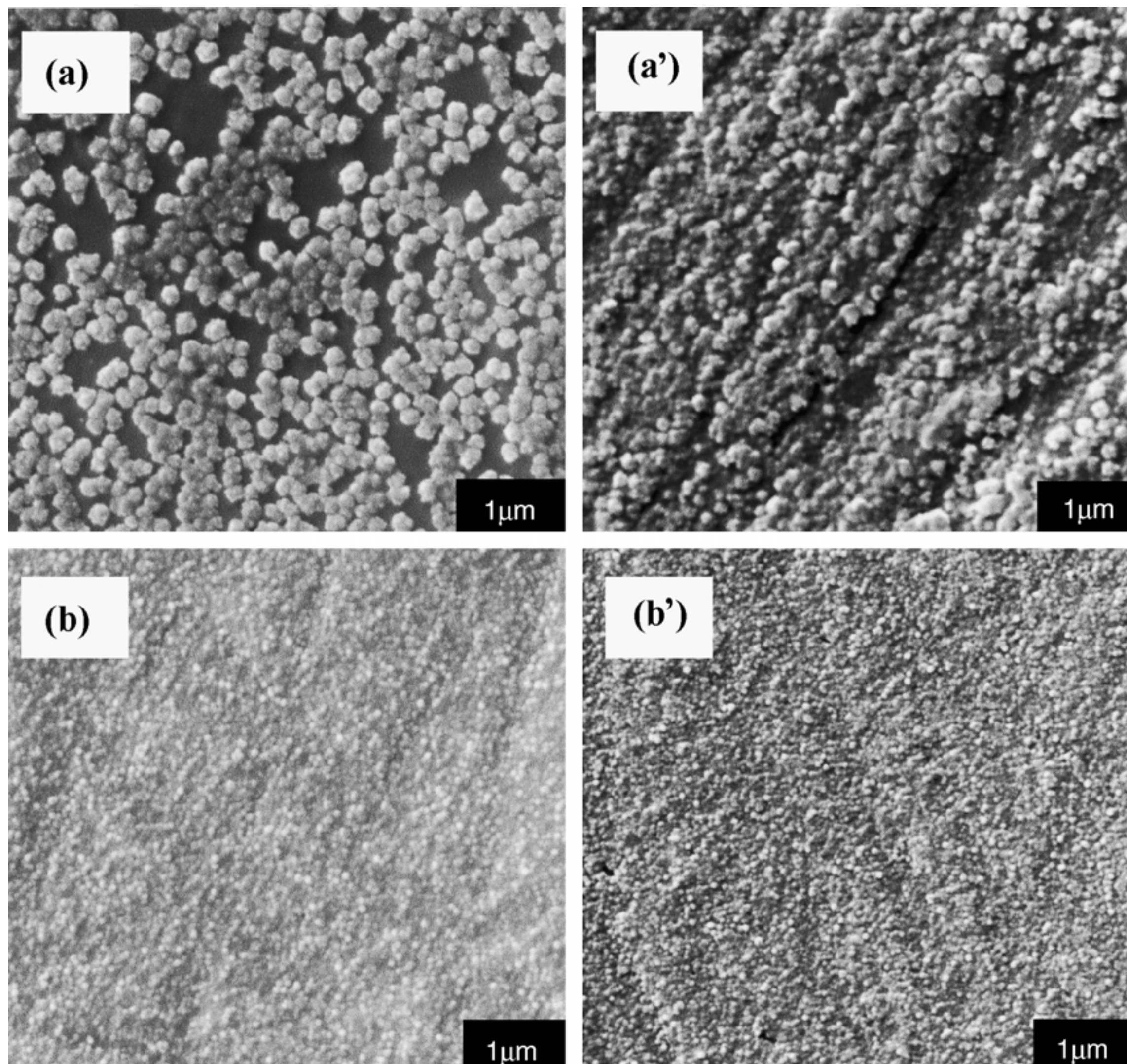


*Fig. 12.* SEM micrographs for Cu films of 0.6 C $cm^{-2}$ obtained chronoamperometrically from −0.3 to −0.69 V ((a) and (a′)) and −0.3 to −1.28 V ((b) and (b′)). Electrolytic solution: 0.10 M $CuSO_4$, 0.20 M $C_3H_8O_3$ and 0.60 M NaOH. $A$=0.5 $cm^2$. Films deposited in absence ((a) ; (b)) and presence ((a′) ; (b′)) of sodium sulfate.

## Acknowledgements

Financial support from Brazilian agencies FAPESP (Proc. 98/10145–4; 99/07414–6) and CAPES is gratefully acknowledged. R.M.Carlos thanks FAPESP for a post doctoral fellowship (Proc. 00/10368–5).

## References

1. V.A. Lamb and D.R. Valentine, *Plating* **52** (1965) 1289.
2. V.A. Lamb and D.R. Valentine, *Plating* **53** (1966) 86.
3. V.A. Lamb, D.R. Valentine and C.E. Johnson, *J. Electrochem. Soc.* **117** (1970) C291, C341.
4. U. Bertoucci and D.R. Turner, *in* A.J. Bard (Ed.), 'Encyclopædia of Elements', (1974) II-6, p. 465.
5. F.A. Lowenheim, 'Modern Electroplating' (J. Wiley & Sons, New York, 1974).
6. N.V. Parthasaradhy, 'Practical Electroplating' (Practice Hall, NJ, 1989).
7. D. Chu and P.S. Fedkiw, *J. Electroanal. Chem.* **345** (1993) 107.
8. R.E. Sinitski, V. Srinivasan and R. Haynes, *J. Electrochem. Soc.* **127** (1980) 47.
9. J. Horner, *Plat. Surf. Finish.* **85**(11) (1998) 42.
10. A.C. Hamilton Jr, *Plat. Surf. Finish.* **85**(11) (1998) 30.
11. J.C. Fabricius, K. Kontturi and G. Sundholm, *J. Appl. Electrochem.* **26** (1996) 1179.
12. Y. Shingaya, H. Matsumoto and M. Ito, *Surf. Sci.* **335** (1995) 23.
13. G. Fabricius, *Electrochim. Acta* **139** (1994) 611.
14. D. Stoychev and C. Tsvetanov, *J. Appl. Electrochem.* **26** (1996) 741.
15. R.Y. Ying, R. Moy, L.C. Fraser, S. O'Bannion and F.M. Donahue, *J. Electrochem. Soc.* **135** (1988) 654.
16. F.M. Donahue, *J. Electrochem. Soc.* **127** (1980) 51.
17. F.M. Donahue, K.L.M. Wong and R. Bhala, *J. Electrochem. Soc.* **127** (1980) 2340.
18. F.M. Donahue, D.J. Sajkowski, A.C. Bosio and L.L. Schafer, *J. Electrochem. Soc.* **129** (1982) 717.
19. M. Matsuoka, J. Murai and C. Iwakura, *J. Electrochem. Soc.* **139** (1992) 2466.
20. L.L. Duda, *Plat. Surf. Finish.* **85**(7) (1998) 60.
21. A. Bettelheim, A. Raveh, U. Mor, R. Ydgar and B. Segal, *J. Electrochem. Soc.* **137** (1990) 3151.
22. R.M. Krishnan, M. Kanagasabapathy, S. Jayakrishnan, S. Sriveeraraghavan, R. Anantharam and S.R. Natarajan, *Plat. Surf. Finish.* **7** (1995) 56.

23. I.A. Carlos and M.M. Oizume, '*Interfinish Latino-Americano EBRATS*-97', São Paulo-SP Brazil (1997) CDROM.
24. V. Alvarez, S. Gonzalez and A. Arevalo, *Electrochim Acta* **29** (1984) 1187.
25. E. Chassaing and K.V. Quang, *J. Appl. Electrochem.* **22** (1986) 591.
26. C. Nila and I. González, *J. Electroanal. Chem.* **401** (1996) 171.
27. N. Sallee, M. Cromer and O. Vittori, *Can. Metall. Q.* **33** (1994) 155.
28. H. Koyano, M. Kato and H. Takenoucki, *J. Electrochem. Soc.* **139** (1992) 3112.
29. I.A. Carlos, C.A.C. Souza, E.M.J.A. Pallone, R.H.P. Francisco, V. Cardoso and B.S. Lima-Neto, *J. Appl. Electrochem.* **30** (2000) 987.
30. I.A. Carlos, M.A. Malaquias, M.M. Oizume and T.T. Matsuo, *J. Power Sources* **92** (2001) 56–64.
31. B.J. Hathaway, *in* 'Comprehensive Coordination Chemistry: the Synthesis, Reactions, Properties and Applications of Coordination Compounds', Vol. 5 (Pergamon Press, New York, 1987).
32. R.G. Pearson, '*Hard and Soft Acids and Bases, HSBA*, *Fundamental Principals Part 1*' **45**(9) (1968) 581.
33. N.S. Isaacs, 'Physical Organic Chemistry' (J. Wiley & Sons, New York, 1987).
34. R.G. Jameson and M.F. Wilson, *J.C.S. Dalton* (1972) 2614.
35. M.A.C. Berton, PhD thesis, Universidade Federal de São Carlos, Brazil (1994).
36. I.A. Carlos, PhD thesis, Universidade Federal de São Carlos, Brazil (1990).
37. A.J. Bard and L.R. Faulkner, 'Electrochemical Methods – Fundamentals and Applications' (J. Wiley & Sons, New York, 1980).
38. A.M.O. Brett and C.M.A. Brett, 'Electroquímica – Princípios, Métodos e Aplicações' (Oxford University Press, New York, 1993).
39. S.E. Group, *in* T.J. Kemp (Ed.), 'Instrumental Methods in Electrochemistry', [Ellis Horwood Series in Physical Chemistry] (John Wiley & Sons, New York, 1985).
40. I.M. Kolthoff and J.J. Lingane, 'Polarography', No. 1 (Interscience, New York, 1952).
41. R.Y. Ying, *J. Electrochem. Soc.* **135**(12) (1988) 2957.
42. S. Fletcher, *Electrochim. Acta* **28**(70) (1983) 971.